Stochastic resonance of ensemble neurons for transient spike trains: Wavelet analysis

Hideo Hasegawa*
Department of Physics, Tokyo Gakugei University, Koganei, Tokyo 184-8501, Japan
(Received 28 November 2001; published 7 August 2002)

By using the wavelet transformation (WT), I have analyzed the response of an ensemble of N ($=1$, 10, 100, and 500) Hodgkin-Huxley neurons to *transient M*-pulse spike trains ($M=1$ to 3) with independent Gaussian noises. The cross correlation between the input and output signals is expressed in terms of the WT expansion coefficients. The signal-to-noise ratio (SNR) is evaluated by using the *denoising* method within the WT, by which the noise contribution is extracted from the output signals. Although the response of a single ($N=1$) neuron to subthreshold transient signals with noises is quite unreliable, the transmission fidelity assessed by the cross correlation and SNR is shown to be much improved by increasing the value of N: a population of neurons plays an indispensable role in the stochastic resonance (SR) for transient spike inputs. It is also shown that in a large-scale ensemble, the transmission fidelity for suprathreshold transient spikes is not significantly degraded by a weak noise which is responsible to SR for subthreshold inputs.

DOI: 10.1103/PhysRevE.66.021902 PACS number(s): 87.10.+e, 84.35.+i, 05.45.−a, 07.05.Mh

I. INTRODUCTION

During the last half century, extensive experimental and theoretical studies have been performed on the functions of brain. However, it remains controversial how neurons communicate information by action potentials or spikes [1–6]. One issue is whether information is encoded in the average firing rate of neurons (*rate code*) or in the precise firing times (*temporal code*). Since Adrian [7] first noted the relationship between neural firing rate and stimulus intensity, the rate-code model has been supported in many experiments of motor and sensory neurons. In the last few years, however, experimental evidences have been accumulated, indicating a use of the temporal code in neural systems; sonar processing of bats [8], sound localization of owls [9], electrosensation in electric fish [10], visual processing of cats [11,12], monkeys [13], and humans [14].

Although many debates on the nature of the neural code have been focused on the rate versus temporal codes, there is another important issue to consider: information is encoded in the activity of single (or very few) neurons or that of a large number of neurons (*population* or *ensemble code*). The population rate-code model assumes that information is coded in the relative firing rates of ensemble neurons, and has been adopted in most of the theoretical analyses. On the contrary, in the population temporal-code model, it is assumed that relative timings between spikes in ensemble neurons may be used as an encoding mechanism for perceptional processing [15–17]. A number of experimental data supporting this code have been reported in recent years [12,18–20]. For example, data have demonstrated that temporally coordinated spikes can systematically signal sensory object feature, even in the absence of changes in firing rate of the spikes [18].

The strong criticism against the temporal code is that spikes are vulnerable to noise while the rate code is robust against noise. It is well known that although firings of single neocortical neurons *in vitro* are precise and reliable, those *in vivo* are quite unreliable [21] due to its noisy environment, which makes the reliability of neurons firings worse. In recent years, however, many studies have been performed for the stochastic resonance (SR) [22,23] in which information transmission of signals is enhanced by background noises. This paradoxical SR phenomenon was first discovered in the context of climate dynamics, and it is now reported in many nonlinear systems such as electric circuits, ring lasers, semiconductor devices, and neurons.

For single neurons, SR has been studied by using various theoretical models such as the integrate-and-fire (IF) model [24–26], the FitzHough-Nagumo (FN) model [27–29], and the Hodgkin-Huxley (HH) model [30]. In these studies, a weak periodic (sinusoidal) signal is applied to the neuron, and it has been reported that the peak height of the interspike-interval (ISI) distribution [24–27] or the signal-to-noise ratio (SNR) of output signals [28–30] shows the maximum when the noise intensity is changed.

SR in coupled or ensemble neurons has been also investigated by using the IF model [31,32], FN model [33–35], and HH model [36–39]. The transmission fidelity is examined by calculating various quantities: the peak-to-width ratio of output signals [31,36,37], the cross correlation between input and output signals [31,33,39], SNR [31,34,39], and the mutual information [35]. One or some of these quantities has been shown to take a maximum as functions of the noise intensity and the coupling strength. Collins, Chow, and Imhoff [33] have pointed out that SR of ensemble neurons is improved as the size of an ensemble is increased. Some physiological experiments support SR in real, biological systems of crayfish [40,41], cricket [42] and rat [43,44].

SR studies mentioned above are motivated from the fact that peripheral sensory neurons play the role of transducers, receiving analog stimuli and emitting spikes. In central neural systems, however, cortical neurons play the role of data processors, receiving and transmitting spike trains. The possibility of SR in the spike transmission has been reported [45–47]. The response to periodic coherent spike-train inputs has been shown to be enhanced by an addition of spike-train

*Email address: hasegawa@u-gakugei.ac.jp

noises characterized by Poisson [45,47] or gamma distribution [46].

It should be stressed that these theoretical studies on SR in neural systems have been performed mostly for stationary analog (or spike-train) signals although they are periodic or aperiodic [33,48]. There have been few theoretical studies on SR for nonstationary signals. Fakir [49] has discussed SR for nonstationary analog inputs with finite duration by calculating the cross correlation. By applying a single impulse, Pei, Wilkinson, and Moss [36] have demonstrated that the spike-timing precision is improved by noises in an ensemble of 1000 HH neurons. One of the reasons why SR study for stationary signals is dominant, is mainly due to the fact that the stationary signals can be easily analyzed by the Fourier transformation (FT) with which, for example, the SNR is evaluated from FT spectra of output signals. The FT requires that a signal to be examined is stationary, not giving the time evolution of the frequency pattern. Actual biological signals are, however, not necessarily stationary. It has been reported that spike signals in cortical neurons are generally not stationary, rather they are transient signals or bursts [50], whereas periodic spikes are found in systems such as auditory system of owl [51] and the electrosensory system of electric fish [52].

The limitation of the FT analysis can be partly resolved by using the short-time Fourier transformation (STFT). Assuming that the signal is quasistationary in the narrow time period, the FT is applied with time-evolving narrow windows. Then STFT yields the time evolution of the frequency spectrum. While the STFT compromise between time and frequency information can be useful, the drawback is that once we choose a particular size of the time window, that window is the same for all frequencies. Many signals require a more flexible approach in which we can vary the window size to determine more accurately either time or frequency.

The drawback of the STFT is overcome in the wavelet transformation (WT) [53,54] with a variable-sized windowing. In contrast to the FT, the WT offers a two-dimensional expansion for a time-dependent signal with the scale and translation parameters which are interpreted physically as the inverse of frequency and time, respectively. The WT allows the use of long time intervals where we want more precise low-frequency information, and shorter regions where we want high-frequency information. As a basis of the WT, we employ the *mother wavelet* which is localized in both frequency and time domains. The WT expansion is carried out in terms of a family of wavelets which is made by dilation and translation of the mother wavelet. The time evolution of frequency pattern can be followed with an optimal time-frequency resolution.

The WT appears to be an ideal tool for analyzing signals of a nonstationary nature. In recent years the WT has been applied to an analysis of biological signals [55], such as electoencephalographic (EEG) waves [56–62], and spikes [63–67]. EEG is a reflection of the activity of ensembles of neurons producing oscillations. By using the WT, we can obtain the time-dependent decomposition of EEG signals to δ (0.3–3.5 Hz), θ (3.5–7.5 Hz), α (7.5–12.5 Hz), β (12.5–30.0 Hz) and γ (30–70 Hz) components [56–62]. It has been shown that the WT is a powerful tool for spike sorting in which coherent signals of a single target neuron are extracted from mixture of response signals [63–65]. Quite recently, Hasegawa [67] has made an analysis of transient spike-train signals of a HH neuron with the use of WT, calculating the energy distribution and Shanon entropy.

It is interesting to analyze the response of ensemble neurons to *transient* spike inputs in a noisy environment by using the WT. There are several sources of noises: (i) cells in sensory neurons are exposed to noises arising from the outer world, (ii) ion channels of the membrane of neurons are known to be stochastic [68], (iii) the synaptic transmission yields noises originating from random fluctuations of the synaptic vesicle release rate [69], and (iv) synaptic inputs include leaked currents from neighboring neurons [70]. Most of the existing studies on SR adopt the Gaussian noises, taking into account the items (i)–(iii). Simulating the noise of the item (iv), Refs. [45–47] include spike-train noises characterized by a Poisson or gamma distribution. In this study we take into account Gaussian noises; SR for spike-train inputs with added spike-train noises will be discussed in a separate paper [71].

We assume an ensemble of HH neurons, which receives transient spike trains consisting of M pulses with added, independent Gaussian noises. The HH neuron model was originally proposed to account for the properties of squid giant axon [72], and it has been generalized with modifications of ion conductances. The HH-type models have been widely adopted for a study of neuronal activity. Neuron models such as the Morris-Lecar [73], FN, and IF models were proposed as the simplified, reduced versions of the HH model. Although these simplified models are more amenable than the HH model, the variables in the models do not have direct empirical basis in real neurons. In this sense, the HH model is known to be the most realistic among theoretical neuron models. The signal transmission is assessed by the cross correlation between input and output signals and SNR, which are expressed in terms of WT expansion coefficients. In calculating the SNR, we adopt the denoising technique within the WT method [74–77], by which the noise contribution is extracted from output signals. The WT denoising method is expected be better than other methods such as Wiener filtering, which is best applied to stationary signals with noises [78].

Our paper is organized as follows. In Sec. II A, an adopted model for an ensemble of N-unit HH neurons is described, and in Sec. II B the WT is briefly discussed. We present the calculated results for $M=1$ pulse train in Sec. III A, and the results for spike trains with $M=2$ and 3 are discussed in Sec. III B. Section IV is devoted to conclusion and discussion.

II. CALCULATION METHODS

A. Ensemble neuron model

We assume a network consisting of N-unit HH neurons which receive the same spike trains but independent Gaussian white noises through excitatory synapses. Spikes emitted by the ensemble neurons are collected by a summing neuron.

A similar model was previously adopted by several authors studying SR for analog signals [33,36,37]. An input signal in this paper is a transient spike train consisting of M impulses ($M=1$ to 3). Dynamics of the membrane potential $V_i(t)$ of the HH neuron i is described by the nonlinear differential equations given by

$$\overline{C}dV_i(t)/dt=-I_i^{\rm ion}(t)+I_i^{\rm ps}(t)+I_i^{\rm n}(t) \quad (\text{for} \quad 1\leqslant i\leqslant N), \tag{1}$$

where $\overline{C}=1\,\mu$F/cm^2 is the capacitance of the membrane. The first term $I_i^{\rm ion}(t)$ of Eq. (1) denotes the ion current given by

$$I_i^{\rm ion}(t)=g_{\rm Na}m_i^3h_i(V_i-V_{\rm Na})+g_{\rm K}n_i^4(V_i-V_{\rm K})+g_L(V_i-V_L), \tag{2}$$

where the maximum values of conductivities of Na and K channels and leakage are $g_{\rm Na}=120$ mS/cm^2, $g_{\rm K}=36$ mS/cm^2, and $g_L=0.3$ mS/cm^2, respectively; the respective reversal potentials are $V_{\rm Na}=50$ mV, $V_{\rm K}=-77$ mV, and $V_L=-54.5$ mV. Dynamics of the gating variables of Na and K channels, m_i, h_i, and n_i, are described by ordinary differential equations, whose details have been given elsewhere [72,79].

The second term $I_i^{\rm ps}(t)$ in Eq. (1) denotes the postsynaptic current given by

$$I_i^{\rm ps}(t)=\sum_{m=1}^{M} g_s(V_a-V_s)\alpha(t-t_{im}), \tag{3}$$

with the alpha function $\alpha(t)$,

$$\alpha(t)=(t/\tau_s)e^{-t/\tau_s}\Theta(t), \tag{4}$$

where the Heaviside function is defined by $\Theta(t)=1$ for $x\geqslant 0$ and 0 for $x<0$, t_{im} is the mth firing time of the input, and g_s, V_s, and τ_s stand for the conductance, reversal potential, and time constant, respectively, of the synapse. The postsynaptic current given by Eq. (3) is induced by an input spike train with the magnitude V_a given by

$$U_i(t)=V_a\sum_{m=1}^{M}\Delta(t-t_{im}), \tag{5}$$

where $\Delta(t)=1$ for $t=0$ and 0 otherwise.

The third term $I_i^n(t)$ in Eq. (1) denotes the Gaussian noise given by

$$\langle\xi_j(t)\rangle=0, \tag{6}$$

$$\langle\xi_j(t)\xi_k(t')\rangle=2D\delta_{jk}\delta(t-t'), \tag{7}$$

where the bracket $\langle X\rangle$ denotes the average and D the intensity of white noises.

The output spike of the neuron i in an ensemble is given by

$$U_{oi}(t)=V_a\sum_n \Delta(t-t_{oin}) \tag{8}$$

in a similar form as an input spike [Eq. (5)], where t_{oin} is the nth firing time when $V_i(t)$ crosses $V_z=0$ mV from below.

We should remark that our model given by Eqs. (1)–(7) does not include couplings among ensemble neurons. This is in contrast with some works on ensemble neurons [34,35,38,39] where introduced couplings among neurons play an important role in SR besides noises, related discussion being given in Sec. IV.

In order to solve stochastic differential equations given by Eqs. (1)–(7), we have adopted the forth-order Runge-Kutta algorithm, which has been widely employed in SR studies, although there are some criticisms that the algorithm is not useful for noisy integration. Our simulations have been performed by the integration time step of 0.01 ms with double precision: some results have been examined by using smaller time steps and also the exponential algorithm. The initial conditions for the variables are given by $V_i(t)=-65$ mV, $m_i(t)=0.0526$, $h_i(t)=0.600$, $n_i(t)=0.313$ at $t=0$, which are the rest-state solution of a single HH neuron. Hereafter, time, voltage, conductance, current, and D are expressed in units of ms, mV, mS/cm^2, μA/cm^2, and μA^2/cm^4, respectively. We have adopted parameters of $V_a=30$, $V_c=-50$, and $\tau_s=\tau_n=2$. Adopted values of g_s, D, M, and N will be described shortly.

B. Wavelet analysis

There are two types of WTs: one is the continuous wavelet transformation (CWT) and the other the discrete wavelet transformation (DWT). In the former the parameters denoting the scale and translation are continuous variables while in the latter they are discrete variables.

The CWT for a given regular function $f(t)$ is defined by

$$c(a,b)=\int dt\,\psi_{ab}^*(t)f(t)\equiv\langle\langle\psi_{ab}(t),f(t)\rangle\rangle, \tag{9}$$

with a family of wavelets $\psi_{ab}(t)$ generated by

$$\psi_{ab}(t)=|a|^{-1/2}\psi\left(\frac{t-b}{a}\right), \tag{10}$$

where $\psi(t)$ is the *mother wavelet*, the asterisk denotes the complex conjugate, and a and b express the scale change and translation, respectively, and they physically stand for the inverse of the frequency and the time. Then the CWT transforms the time-dependent function $f(t)$ into the frequency- and time-dependent function $c(a,b)$. The mother wavelet is a smooth function with good localization in both frequency and time spaces. A wavelet family given by Eq. (10) plays a role of elementary function, representing the function $f(t)$ as a superposition of wavelets $\psi_{ab}(t)$.

The *inverse* of the wavelet transformation may be given by

$$f(t)=C_\psi^{-1}\int\frac{da}{a^2}\int dbc(a,b)\psi_{ab}(t) \tag{11}$$

when the mother wavelet satisfies the following two conditions: (i) the admissibility condition given by

$$0<C_{\psi}<\infty, \tag{12}$$

with

$$C_{\psi}=\int_{-\infty}^{\infty} d\omega|\hat{\Psi}(\omega)|^2/|\omega|, \tag{13}$$

where $\hat{\Psi}(\omega)$ is the Fourier transformation of $\psi(t)$, and (ii) the zero mean of the mother wavelet,

$$\int_{-\infty}^{\infty} dt\psi(t)=\hat{\Psi}(0)=0. \tag{14}$$

On the contrary, the DWT is defined for *discrete* values of $a=2^j$ and $b=2^j k$ (j,k: integers) as

$$c_{jk}\equiv c(2^j,2^j k)=\langle\langle\psi_{jk}(t),f(t)\rangle\rangle, \tag{15}$$

with

$$\psi_{jk}(t)=2^{-j/2}\psi(2^{-j}t-k). \tag{16}$$

The orthonormal condition for the wavelet functions is given by

$$\ll\psi_{jk}(t),\psi_{j'k'}(t)\gg=\delta_{jj'}\delta_{kk'}, \tag{17}$$

leading to the inverse DWT,

$$f(t)=\sum_j f_j(t)\simeq\sum_{j\leqslant J} f_j(t)\equiv f_I(t), \tag{18}$$

with

$$f_j(t)=\sum_k c_{jk}\psi_{jk}(t), \tag{19}$$

where $f_I(t)$ stands for an approximate function generated by inverse DWT with J, the adopted maximum value of j.

In the multiresolution analysis of the DWT, we introduce a scaling function $\phi(t)$, which satisfies the recurrent relation with $2K$ masking coefficients, h_k, given by

$$\phi(t)=\sqrt{2}\sum_{k=0}^{2K-1} h_k\phi(2t-k), \tag{20}$$

with the normalization condition for $\phi(t)$ given by

$$\int dt\phi(t)=1. \tag{21}$$

A family of wavelet functions is generated by

$$\psi(t)=\sqrt{2}\sum_{k=0}^{2K-1}(-1)^k h_{2K-1-k}\phi(2t-k). \tag{22}$$

The scaling and wavelet functions satisfy the orthonormal relations,

$$\langle\langle\phi(t),\phi(t-m)\rangle\rangle=\delta_{m0}, \tag{23}$$

$$\langle\langle\psi(t),\psi(t-m)\rangle\rangle=\delta_{m0}, \tag{24}$$

$$\langle\langle\phi(t),\psi(t-m)\rangle\rangle=0. \tag{25}$$

A set of masking coefficients h_j is chosen so as to satisfy the conditions shown above.

The simplest wavelet function for $K=1$ is the Harr wavelet for which we get $h_0=h_1=1/\sqrt{2}$, and

$$\begin{aligned}\psi_H(t)&=1 \quad \text{for} \quad 0\leqslant t<1/2\\ &=-1 \quad \text{for} \quad 1/2\leqslant t<1\\ &=0 \quad \text{otherwise.}\end{aligned} \tag{26}$$

In the more sophisticated wavelets like the Daubechies wavelet, an additional condition given by

$$\int dtt^l\psi(t)=0 \quad \text{for} \quad l=0,1,2,3,\ldots,L-1 \tag{27}$$

is imposed for the smoothness of the wavelet function. Furthermore, in the Coiflet wavelet, for example, a similar smoothing condition is imposed also for the scaling function as

$$\int dtt^l\phi(t)=0 \quad \text{for} \quad l=1,2,3,\ldots,L-1. \tag{28}$$

Once WT coefficients are obtained, we can calculate various quantities such as autocorrelation, cross correlations, and SNR, as will be discussed shortly. In principle, the expansion coefficients c_{jk} in DWT may be calculated by using Eqs. (15) and (16) for a given function $f(t)$ and an adopted mother wavelet $\psi(t)$. This integration is, however, inconvenient, and in an actual fast wavelet transformation, the expansion coefficients are obtained by a matrix multiplication with the use of the iterative formulas given by the masking coefficients and expansion coefficients of the neighboring levels of indices, j and k [54].

One of the advantages of the WT over FT is that we can choose a proper mother wavelet among many mother wavelets, depending on the signal to be analyzed. Among many candidates of mother wavelets, we have adopted the Coiflet 4 with the resolution level of $J=5$, forming a compromise between the accuracy and the computational effort (the shape of the adopted mother wavelet is realized in Fig. 8.3 of Ref. [53]). The WT has been performed by using the MATLAB wavelet tool box and FORTRAN programs with some modifications [80]. As will be shown shortly, the transformation error defined by $\epsilon\equiv\|f_I-f\|/\|f\|$ is of the order of 10^{-12} where $\|f\|=\sqrt{\int dt|f(t)|^2}$, and $f(t)$ and $f_I(t)$ are original and (approximate) inverse DWT signals, respectively [Eq. (18)].

III. CALCULATED RESULTS

A. Input pulses with $M=1$

First we discuss the case in which ensemble HH neurons receive a common single ($M=1$) impulse. When input syn-

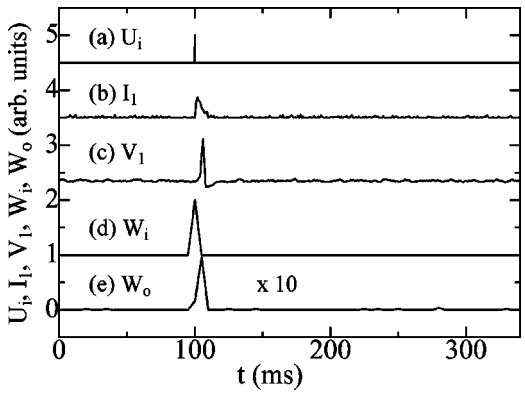

FIG. 1. The time dependence of (a) the $M=1$ input pulse (U_i), (b) the postsynaptic current ($I_1=I_1^{ps}+I_1^n$), (c) the membrane potential of the neuron $I=1$ (V_1), and (d) input (W_i), and (e) output signals ($W_o\times 10$) with the time bin of $T_b=5$ ms for $D=0.5$, $g_s=0.06$, and $N=500$. The vertical scale is only for W_i and W_o (W_i is shifted upwards by 1.0).

aptic strength is small ($g_s<g_{th}$), no neurons fire in the noise-free case, while if it is sufficiently large ($g_s\geqslant g_{th}$), all neurons fire where $g_{th}=0.091$ is the threshold value. For a while, we will discuss the subthreshold case of $g_s=0.06<g_{th}$ with $N=500$. The $M=1$ input pulse is applied at $t=100$ ms, as shown in Fig. 1(a). Figure 1(b) shows the time dependence of the postsynaptic current, $I_i(t)=I_i^{ps}(t)+I_i^n(t)$, of the neuron $i=1$ with added noises of $D=0.5$. The states of neurons when they receive input pulse are randomized [37] because noises have been already applied before a $M=1$ signal. Figure 1(c) shows the time dependence of the membrane potential $V_1(t)$ of the neuron 1, which fires with a delay of about 6 ms. This delay time is much larger than the conventional value of 2–3 ms for suprathreshold inputs, because marginal, subthreshold inputs with small noises at synapses need a fairly long integration period before firings [79].

Firings in ensemble 500 neurons for $D=0.5$ are depicted by raster in Fig. 2(a). We note that neurons fire not only by input pulses plus noises but also spuriously by noises only. When the noise intensity is increased to $D=1.0$, spurious firings are much increased, as shown in Fig. 2(b), where a firing delay time is reduced to about 2–3 ms, almost the same as the conventional value [79].

We will study how information is transmitted through ensemble HH neurons with the use of the DWT, assuming that information is carried by firing times of spikes but not by details of their shapes. Just as the first Fourier transformation, DWT requires input data to be given at discrete points with equal spacing. Then we divide the time scale by the width of time bin of T_b in order to define the input and output signals at discrete times as

$$W_i(t)=\sum_l \sum_m \Theta(T_b/2-|t-t_{im}|)\Delta(t-lT_b), \quad (29)$$

$$W_o(t)=(1/N)\sum_{i=1}^{N} \sum_l \sum_n \Theta(T_b/2-|t-t_{oin}|)\Delta(t-lT_b). \quad (30)$$

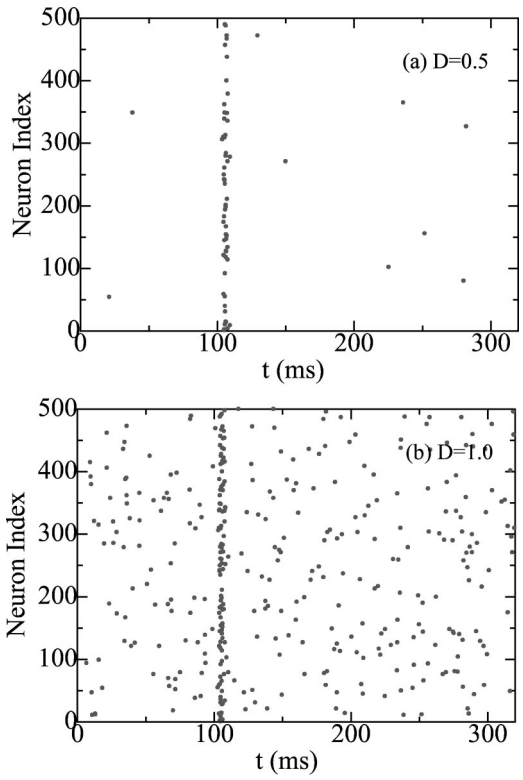

FIG. 2. Rasters showing firings in ensemble neurons for (a) $D=0.5$ and (b) $D=1.0$ with $M=1$, $g_s=0.06$, and $N=500$.

In Eqs. (29) and (30) $W_i(t)$ stands for the external input signal (without noises), $W_o(t)$ the output signal averaged over the ensemble neurons, $\Theta(t)$ the Heaviside function, $\Delta(t)=1$ for $t=0$ and 0 otherwise, t_{im} the mth firing time of inputs, and t_{oin} the nth firing time of outputs of the neuron i [Eq. (8)]. Our simulation has tentatively adopted the time bin of $T_b=5$ ms, which is comparable to the characteristic time constant of neurons. A single simulation has been performed for 320 ($=2^6T_b$) ms. A $M=1$ input pulse at $t=100$ ms leads to $W_i(t=100)=1.0$ in Eq. (29). $W_i(t)$ is shown in Fig. 1(d) where the function defined by Eq. (29) at the discrete times of lT_b are connected by lines. Figure 1(e) similarly shows $W_o(t)$ for the case of $D=0.5$. The magnitude of $W_o(t)$ is much smaller than that of $W_i(t)$ because only a few neurons fire among 500 neurons: note that the curve in Fig. 1(e) is multiplied by a factor of ten. Figure 1(e) shows that firings by input signal plus noise yield $W_o(t=100)=0.016$ and $W_o(t=105)=0.096$, and noise-only firings yield small contributions to $W_o(t)$. The peak position of $W_o(t)$ is slightly shifted compared to that of $W_i(t)$ because of a delay of neuron firings as mentioned above.

1. Wavelet transformation

Now we apply the DWT to input and output signals. By substituting $f(t)=W_i(t)$ or $W_o(t)$ in Eq. (15), we get their WT coefficients given by

$$c_{\lambda jk}=\int dt\,\psi_{jk}^*(t)W_\lambda(t) \quad (\lambda=i,o), \quad (31)$$

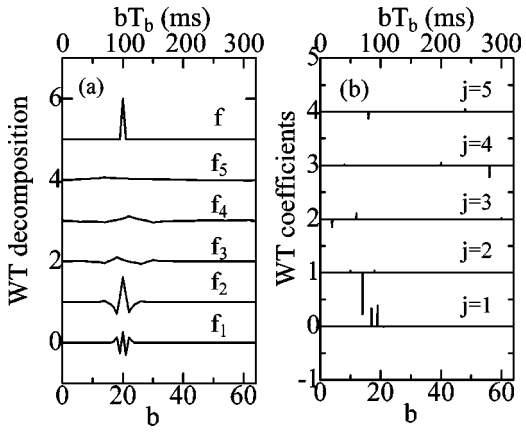

FIG. 3. (a) The input signal $f=W_i$ (uppermost frame) for $M=1$ with WT decomposition: $f\simeq\Sigma_{j=1}^{5}f_j$, and (b) its WT expansion coefficients c_{jk}. Curves of f_j for $j\geqslant 2$ and f in (a), and those of c_{jk} for $j\geqslant 2$ in (b) are successively shifted upward by 1.0. Upper horizontal scale expresses bT_b in ms.

where $\psi_{jk}(t)$ is a family of wavelets generated from the mother Coiflet wavelet [see Eq. (16)]. The uppermost frame of Fig. 3(a) expresses the input signal $W_i(t)$. Note that the lower and upper horizontal scales express b and bT_b (in units of ms), respectively. Figure 3(b) shows the calculated WT coefficients of $W_i(t)$ which are plotted as a function of $b(j,k)=(k-0.5)2^j$ for various j values after convention. The WT coefficients of $j=1$ and 2 have large values near $b=20$ ($bT_b=100$ ms) where $W_i(t)$ has a peak. Contributions from $j=1$ and $j=2$ are predominant in $W_i(t)$. It is noted that the WT coefficient for $j=4$ has a significant value at $b\sim 56$ far away from $b=20$. The decomposition of the inverse WT signal: $f(t)\simeq f_I(t)=\Sigma_{j=1}^{5}f_j(t)$ [Eq. (18)] is plotted in Fig. 3(a). The transformation error is $\epsilon\equiv\|f_I-f\|/\|f\|\sim 2.12\times 10^{-12}$, and then the inverse WT function $f_I(t)$ shows good agreement with the original function $f(t)$. The WT decomposition for output signal $W_o(t)$ for $D=0.5$ are shown in Fig. 4(a), in which the transformation error is $\epsilon\sim 2.03\times 10^{-12}$. The WT coefficients depicted in Fig. 4(b) show the dominant contribution to arise from $j=1$ in $W_o(t)$. Similar plots of the WT decomposition and the WT coefficients of the output signal $W_o(t)$ for $D=1.0$ are presented in Figs. 5(a) and 5(b), respectively. The denosing technique employed in Figs. 4(c), 4(d), 5(c), and 5(d) will be explained later. An input pulse plus noise yield the output signal with $W_o(t=100)=0.088$ and $W_o(t=105)=0.126$, for which the transformation error is again very small: $\epsilon\sim 1.96\times 10^{-12}$. As the noise intensity is increased, fine structures in the WT coefficients appear, in particular for small j.

2. Autocorrelation and cross correlations

The autocorrelation functions for input (Γ_{ii}) and output signals (Γ_{oo}) are defined by

$$\Gamma_{\lambda\lambda}=M^{-1}\int dtW_\lambda(t)^*W_\lambda(t)$$

$$=M^{-1}\sum_j\sum_k c_{\lambda jk}^*c_{\lambda jk}\quad(\lambda=i,o),\tag{32}$$

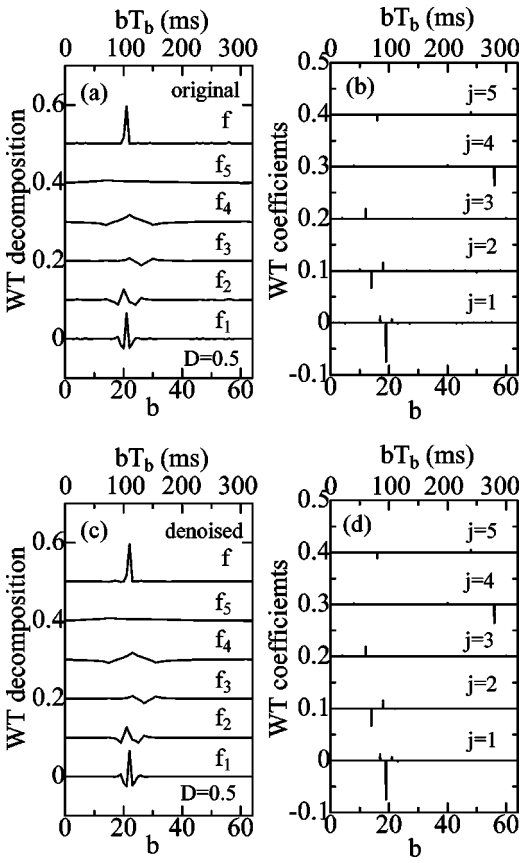

FIG. 4. (a) The original output signal $f=W_o$ (uppermost frame) for $D=0.5$ and $M=1$ with its WT decomposition: $f\simeq\Sigma_{j=1}^{5}f_j$, and (b) its WT expansion coefficients c_{jk}. (c) The denoised output signal (uppermost frame) with WT decomposition, and (d) its WT expansion coefficients c_{jk}^{dn} denoised with the parameters of $j_c=3$ and $\delta b=5$. Curves of f_j for $j\geqslant 2$ and f in (a) and (c), and those of c_{jk} for $j\geqslant 2$ in (b) and (d) are successively shifted upward by 0.1. Upper horizontal scale expresses bT_b in ms.

where the orthonormal relations of the wavelets given by Eqs. (23)–(25) are employed. Similarly the cross correlation between input and output signals is defined by

$$\Gamma_{io}(\beta)=M^{-1}\int dtW_i(t)^*W_o(t+\beta T_b)$$

$$=M^{-1}\sum_j\sum_k c_{ijk}^*c_{ojk}(\beta),\tag{33}$$

where c_{ijk} and $c_{ojk}(\beta)$ are the expansion coefficients of $W_i(t)$ and $W_o(t+\beta T_b)$, respectively. We define the maximum in the input-output correlation by

$$\Gamma=\max_\beta[\Gamma_{io}(\beta)],\tag{34}$$

and that in the normalized cross correlation by

$$\gamma=\max_\beta\left[\frac{\Gamma_{io}(\beta)}{\sqrt{\Gamma_{ii}}\sqrt{\Gamma_{oo}}}\right]=\frac{\Gamma}{\sqrt{\Gamma_{ii}}\sqrt{\Gamma_{oo}}}.\tag{35}$$

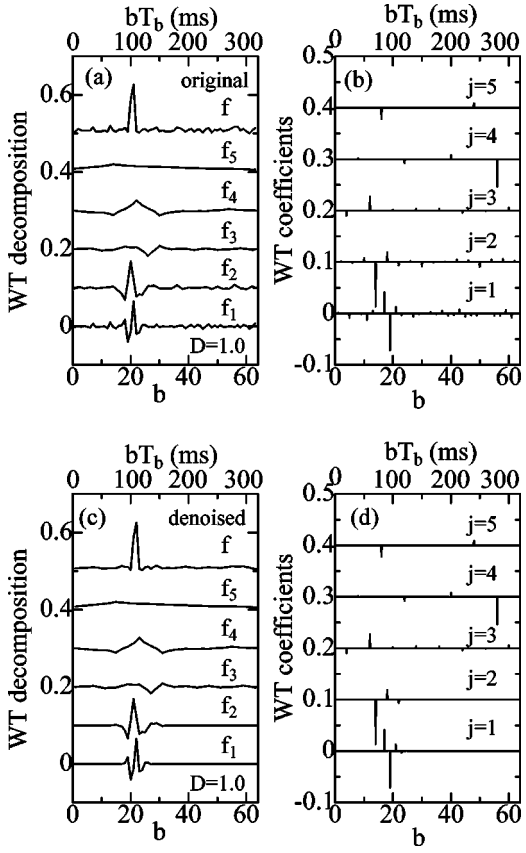

FIG. 5. (a) The original output signal $f=W_o$ (uppermost frame) for $D=1.0$ and $M=1$ with its WT decomposition: $f\simeq\Sigma_{j=1}^{5}f_j$, and (b) its WT expansion coefficients c_{jk}. (c) The denoised output signal (uppermost frame) with WT decomposition, and (d) its WT expansion coefficients c_{jk}^{dn} denoised with the parameters of $j_c=3$ and $\delta b=5$. Same as in Fig. 4.

It is noted that for the suprathreshold inputs in the noise-free case, we get $\Gamma_{oo}=\Gamma_{io}=1$ and then $\Gamma=\gamma=1$ $(\Gamma_{ii}=1)$.

Figure 6(a) shows the D dependence of Γ, Γ_{oo}, and γ for $g=0.06$ and $N=500$. They are zero at $D=0$ because of the adopted subthreshold parameters. Upon increasing D from zero, Γ and Γ_{oo} increase gradually, but γ increases rapidly as clearly shown in the left panel where we plot the result for the narrow range of $0\leqslant D\leqslant 0.2$, marked by vertical, dashed line in the right panel. Because of the factor of $1/\sqrt{\Gamma_{oo}}$ in Eq. (35), the magnitude of γ is larger than that of Γ. We note that γ is enhanced by weak noises and it is decreased at larger noises, which is a typical SR behavior.

3. Signal-to-noise ratio

We will evaluate the SNR by employing the denoising method [74–77]. The key point in the denoising is how to choose which wavelet coefficients are correlated with the signal and which ones with noises. The simple denoising method is to neglect some DWT expansion coefficients when reproducing the signal by the inverse wavelet transformation. We get the denoised signal by the inverse WT [Eq. (18)],

$$W_{\lambda}^{dn}(t)=\sum_{j}\sum_{k}c_{\lambda jk}^{dn}\psi_{jk}(t), \tag{36}$$

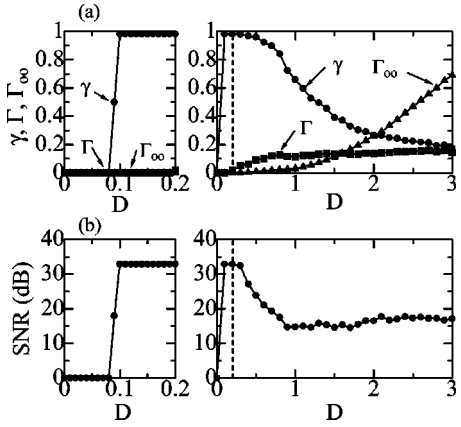

FIG. 6. The D dependence of (a) γ (circles), Γ_{oo} (triangles), and Γ (squares), and (b) SNR for $M=1$, $g_s=0.06$, and $N=500$. Left panels of (a) and (b) show the enlarged plots of right panels of (a) and (b), respectively, in the narrow range of $0\leqslant D\leqslant 0.2$ marked by vertical, dashed lines.

with the denoised WT coefficients c_{jk}^{dn} to be chosen properly as will be discussed below. The simplest denoising method, for example, is to assume that WT components for $a<a_c$ in the (a,b) plane arise from noises to set the denoised WT coefficients as

$$\begin{aligned} c_{jk}^{dn}&=c_{jk} \quad \text{for} \quad j\geqslant j_c \quad (a\geqslant a_c)\\ &=0 \qquad \text{otherwise,}\end{aligned} \tag{37}$$

where j_c $(=\log_2 a_c)$ is the critical j value [74].

In our simulation we adopt a more sophisticated method. Assuming that the components for $b<b_L$ or $b>b_U$ at $a<a_c$ in the (a,b) plane are noises, we set the denoised WT coefficients as

$$\begin{aligned} c_{jk}^{dn}&=c_{jk} \quad \text{for} \quad j\geqslant j_c \quad \text{or} \quad k_L\leqslant k\leqslant k_U\\ &=0 \qquad \text{otherwise,}\end{aligned} \tag{38}$$

where j_c $(=\log_2 a_c)$ denotes the critical j value, and k_L $(=b_L 2^{-j})$ and k_U $(=b_U 2^{-j})$ are the lower and upper critical k values, respectively, for $j<j_c$. We will obtain the inverse, denoised signal by using Eq. (36) with the denoised WT coefficients determined by Eq. (38).

In the present case we can fortunately obtain the WT coefficients for *ideal* case of noise-free and suprathreshold inputs. We then properly determine the denoising parameters of j_c, b_L, and b_U. From the observation of the WT coefficients for the ideal case, which is not shown here but is not dissimilar to those shown in Figs. 3(a) and 4(a), we assume that the upper and lower bounds may be chosen as

$$b_L=t_{o1}/T_b-\delta b_L, \quad b_U=t_{oM}/T_b+\delta b_U, \tag{39}$$

where t_{o1} (t_{oM}) are the first $(M\text{th})$ firing times of output signals in the ideal case of noise-free and suprathreshold inputs, and δb_L and b_U denote the marginal distances from the b values expected to be responsible to the signal transmis-

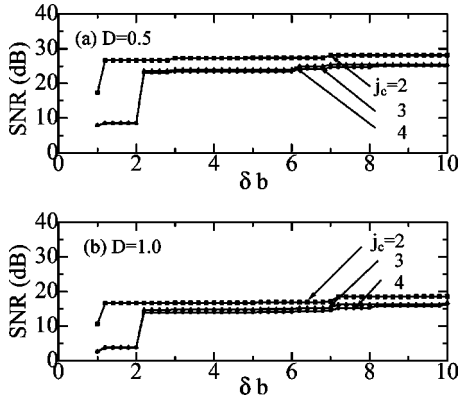

FIG. 7. The δb dependence of SNR of output signals for (a) $D=0.5$ and (b) $D=1.0$ with $j_c=2$ (squares), 3 (triangles), and 4 (circles) for $M=1$, $g_s=0.06$, and $N=500$ (see text).

sion. In order to reduce the number of parameters, we set $\delta b_L=\delta b_U=\delta b$, although a choice of parameters with $\delta b_L<\delta b_U$ may be better when a transmission delay of neurons is taken into account.

From the above consideration, we may define the signal (A_s) and noise components (A_n) by

$$A_s=\int dt W_o^{dn}(t)^* W_o^{dn}(t)=\sum_j \sum_k |c_{ojk}^{dn}|^2, \qquad (40)$$

$$A_n=\int dt[W_o(t)^* W_o(t)-W_o^{dn}(t)^* W_o^{dn}(t)]$$

$$=\sum_j \sum_k (|c_{ojk}|^2-|c_{ojk}^{dn}|^2). \qquad (41)$$

The SNR, η, is defined by

$$\eta=10\ \log_{10}(A_s/A_n)\quad (\mathrm{dB}). \qquad (42)$$

Figure 4(d) shows the denoised WT coefficients c_{jk}^{dn} when the WT coefficients c_{jk} of the original output signal for $D=0.5$ shown in Fig. 1(b), are denoised by using Eqs. (38) and (39) with parameters of $j_c=3$ and $\delta b=5$. WT coefficients for $j<3$ and $|b-20|>5$ ($|bT_b-100|>25$ ms) are set zero after the denoising condition [Eq. (38)]. The denoised signal of W_o^{dn}, which is given by Eq. (36) and which is shown in Fig. 4(c), is almost the same as the original signal shown in Fig. 4(a). The denoised WT coefficient for $D=1.0$ with the same denoising parameters of $j_c=3$ and $\delta b=5$, is depicted in Fig. 5(d). The denoised WT signal of W_o^{dn} shown in Fig. 5(c) has less amount of ripples than the original signal shown in Fig. 5(a).

In order to investigate the effect of denosing parameters, j_c and δb, on denoised signals, we have calculated SNR η defined by Eq. (42) by changing these parameters. Figures 7(a) and 7(b) show the δb dependence of SNR of W_o for $D=0.5$ and $D=1.0$, respectively, calculated with various j_c values. We note that an increase in j_c and/or a decrease in δb reduce SNR because of increased noise contributions [Eq. (41)]. We have decided to adopt $j_c=3$ and $\delta b=5$ for our simulations.

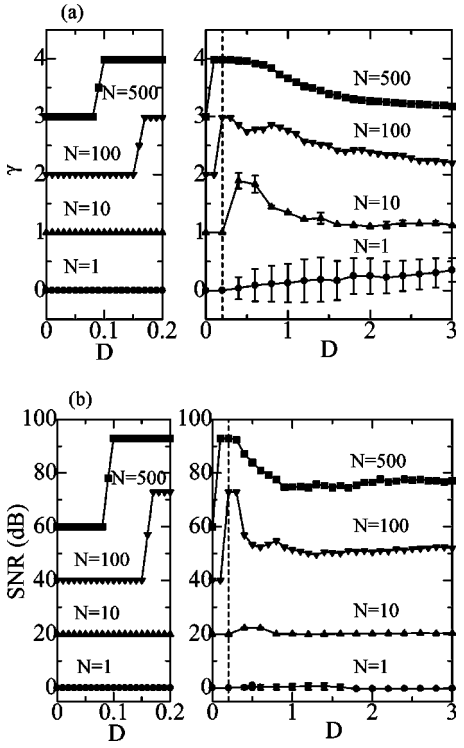

FIG. 8. (a) The cross correlation γ and (b) SNR as a function of D for $M=1$ and $g_s=0.06$ with $N=1$, 10, 100, and 500. Left panels of (a) and (b) show the enlarged plots of right panels of (a) and (b), respectively, in the narrow range of $0\leqslant D\leqslant 0.2$ marked by vertical, dashed lines. Results for $N=1$ ($N=10$) are averaged values of 100 (10) trials and their rms is shown by error bars. Results of (a) and (b) for $N=10$, 100, and 500 are successively shifted upward by 1.0 and 20, respectively.

The D dependence of SNR calculated for $g=0.06$ and $N=500$ is plotted in Fig. 6(b), where the left panel shows the enlarged plot of the right panel in the narrow range of $0\leqslant D\leqslant 0.2$ marked by the vertical, dashed line. We note that SNR shows a typical SR behavior: a rapid rise to a clear peak and a slow decrease for larger D value.

So far, our simulation has been made for the fixed parameters of $g_s=0.06$ and $N=500$, which will be changed in the followings. By adopting $N=1$, 10, 100, and 500, we have obtained the D dependence of the cross correlation γ and SNR plotted in Figs. 8(a) and 8(b), respectively, where left panels show the enlarged plots of the right panels in the narrow range of $0\leqslant D\leqslant 0.2$ marked by vertical, dashed lines. Results for $N=1$ and 10 are averaged values of hundred and ten trials, respectively, while those for $N=100$ and 500 are of single runs. The results of $N=500$ show the typical SR behavior as mentioned before [Figs. 6(a) and 6(b)]. On the contrary, SR effect for a single $(N=1)$ neurons is marginally realized in SNR but not in γ. Large error bars for the results of $N=1$ imply that the reliability of information transmission is very low in the subthreshold condition [21]. This is clearly seen in Figs. 9(a) and 9(b) where γ and SNR for

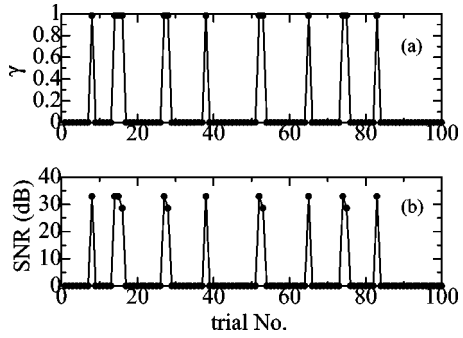

FIG. 9. (a) The cross correlation γ and (b) SNR of 100 trials for single ($N=1$) neurons with $D=1.0$, $g_s=0.06$, and $M=1$.

$D=1.0$ with $N=1$ are plotted against the trial number of 100 runs. The signal can be transmitted only when the signal fortunately coincides with noises and the signal plus noise crosses the threshold level. Then only 13 among 100 trials are succeeded in the transmission of $M=1$ inputs through a neuron. We note in Figs. 8(a) and 8(b) that as the size of the network is much increased, the peak values of γ and SNR are much enhanced and the SR behavior becomes more evident. Figures 8(a) and 8(b) demonstrate that the ensemble of neurons play an *indispensable* role in information transmission of transient spike signals. This is consistent with the results of Collins *et al.* [33] and Pei *et al.* [36], who have pointed out the improvement of the information transmission by increasing the size of the network.

Next we change the value of g_s, the strength of input synapses. The g_s dependence of γ and SNR for $N=500$ neurons is shown in Figs. 10(a) and 10(b), respectively, where values of $D=0.0$, 0.5, and 1.0 are employed. Note that in the noise-free case ($D=0$), we get $\gamma=1$ and SNR$=\infty$ for $g_s \geqslant g_{th}$ but $\gamma=0$ and SNR$=-\infty$ for $g_s<g_{th}$, as shown by dotted curves in Figs. 10(a) and 10(b). It is shown that moderate subthreshold noises considerably improve the transition fidelity. For a comparison, the g_s dependence of γ and SNR for single ($N=1$) neurons is shown in Figs. 11(a) and 11(b), respectively. As has been shown in Fig. 8(a), SR for $N=1$ is

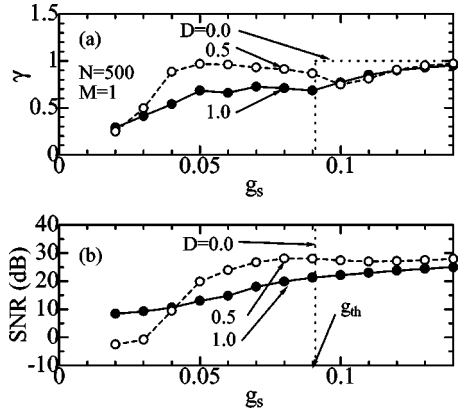

FIG. 10. The g_s dependence of the cross correlation γ and SNR for $N=500$ and $M=1$. Dotted, dashed, and solid curves denote the results of $D=0.0$, 0.5, and 1.0, respectively. The arrow expresses the threshold g_s value.

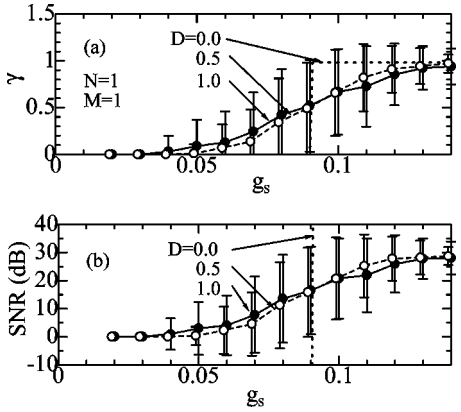

FIG. 11. The g_s dependence of the cross correlation γ and SNR for $N=1$ and $M=1$. Dotted, dashed, and solid curves denote the results of $D=0.0$, 0.5, and 1.0, respectively, and error bars express rms values for 100 trials.

less significant compared to that for $N=500$. We note that the g_s dependence of γ for $N=500$ in Fig. 10(a) is not monotonic, while that for $N=1$ in Fig. 11(a) is monotonic. This is expected to be due to small fluctuations in calculated results of $N=500$, for which single runs may be insufficient to get monotonic, regular results: the monotonic result of $N=1$ is the average of hundred runs. The reason why the result of γ is more irregular than that of SNR in Fig. 10 is not clear at the moment. It should be noted in Figs. 10(a) and 10(b) that the presence of weak noises does not significantly degrade the transmission fidelity for suprathreshold cases in ensemble neurons.

B. Input pulses with $M=2$ and 3

Now we discuss the cases of $M=2$ and 3. Input pulses are applied at $t=100$ and 125 ms for the $M=2$ case. The ISI of input signal is assume to be $T_i=25$ ms because spikes with this value of ISI are reported to be ubiquitous in cortical brains [50]. Firings of 500 neurons for the noise intensity of $D=1.0$ are shown by raster in Figs. 12(a), which shows that firings occur mainly at $t\sim 103$ and 128 ms with a delay of about 3 ms. The output signal $W_o(t)$ averaged over $N=500$ neurons is depicted by the solid curve in the uppermost frame of Fig. 13(a), which has two main peaks. The WT decomposition and WT coefficients of $W_o(t)$ are plotted in Figs. 13(a) and 13(b), respectively. When we compare the results for $M=2$ shown in Figs. 13(a) and 13(b) with those for $M=1$ shown in Figs. 5(a) and 5(b), we note that components for $j=1$ and 2 for $M=2$ are much increased because of the presence of the second peak for $M=2$ inputs while the contributions from $j\geqslant 3$ are changed little. The denoising has been made by the procedure given by Eqs. (36), (38), and (39) with parameters of $j_c=3$ and $\delta b=5$. WT decomposition of a denoised signal and denoised WT coefficients are shown in Figs. 13(c) and 13(d), respectively.

Similarly we apply the $M=3$ pulse at $t=100$, 125, and 150 ms, the input ISI being again $T_i=25$ ms. Raster in Fig. 12(b) shows firing of 500 neurons for $D=1.0$. Firings mainly occur at $t\sim 103$, 128, and 153 ms with a delay of about 3 ms.

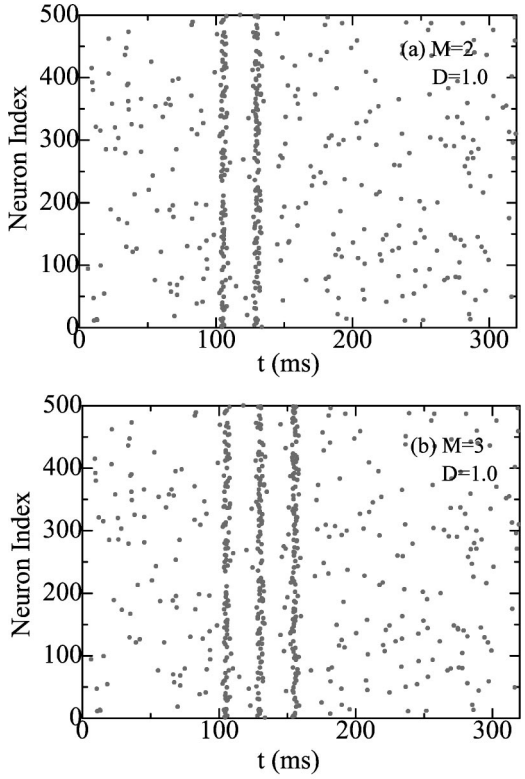

FIG. 12. Raster showing firings in ensemble neurons for (a) $M=2$ and (b) $M=3$ with $D=1.0$, $g_s=0.06$, and $N=500$.

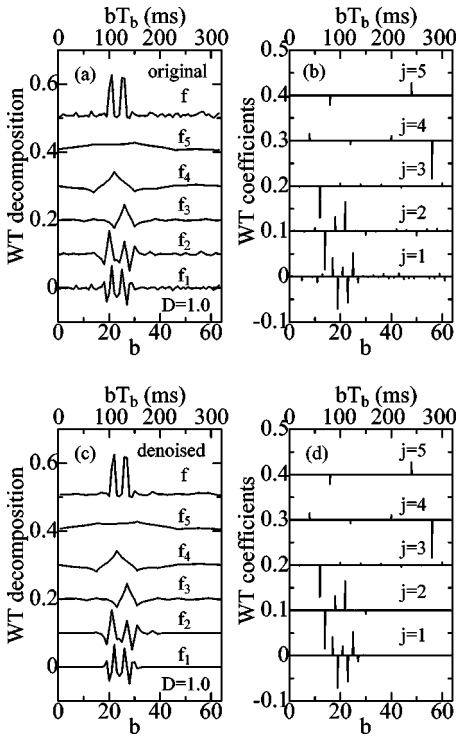

FIG. 13. (a) The original output signal $f=W_o$ (uppermost frame) for $D=1.0$ and $M=2$ with WT decomposition: $f\simeq\Sigma_{j=1}^{5}f_j$ and (b) its WT expansion coefficients c_{jk}. (c) The denoised output signal (uppermost frame) with WT decomposition, and (d) its WT expansion coefficients c_{jk}^{dn} denoised with the parameters of $j_c=3$ and $\delta b=5$. Curves of f_j for $j\geqslant 2$ and f in (a) and (c), and those of c_{jk} for $j\geqslant 2$ in (b) and (d) are successively shifted upward by 0.1. Upper horizontal scale expresses bT_b in ms.

The solid curve in the uppermost frame of Fig. 14(a) shows the averaged output of $W_o(t)$ for $D=1.0$. The solid bars in Fig. 14(b) show its WT coefficients and the solid curves in Fig. 14(a) express its WT decomposition. Again, components of $j=1$ and 2 are much increased because of the second and third peaks in $W_o(t)$. Figures 14(c) and 14(d) show WT decomposition of a denoised signal and denoised WT coefficients, respectively.

The calculated D dependence of the cross correlation γ (SNR) for $M=1$, 2, and 3 is plotted in Fig. 15(a) [Fig. 15(b)]. Both γ and SNR show typical SR behavior irrespective of the value of M, although a slight difference exists between the M dependence of γ and SNR: for larger M, the former is larger but the latter is smaller at the moderate noise intensity of $D<1.0$. When similar simulations are performed for different ISI values of $T_i=15$ and 35 ms, we obtain results which are almost the same as that for $T_i=25$ (not shown). This is because the output spikes for inputs with $M=2$ and 3 are superposition of an output spike for a $M=1$ input when input ISI is larger than the refractory period of neurons (~ 10 ms).

IV. CONCLUSION AND DISCUSSION

Our simulations based on the temporal-code model have shown that a population of neurons plays a very important role in the transmission of subthreshold transient spike signals [Figs. 8(a) and 8(b)]. In particular, for single neurons the transmission is quite unreliable and the appreciable SR effect is not realized. When the size of ensemble neurons is increased, the transmission fidelity is much improved in a fairly wide range of the g_s parameter for both the subthreshold and suprathreshold cases (Fig. 10). We note in Figs. 8(a) and 8(b) that γ (or SNR) for $N=100$ with a single run is different from and larger than that for $N=1$ with 100 runs. This seems strange because if there is no couplings among neurons as in our model, a simulation for an ensemble of N neurons with a single trial is expected to be equivalent to simulations for a single neuron with N trials. This is, however, not true, and it will be understood as follows. We consider a quantity of $X(N,N_r)$ which is γ (or SNR) averaged over N_r trials for an ensemble of N neurons. We implicitly express $X(N,N_r)$ as

$$X(N,N_r)=\langle\langle F(\langle w_i^{(\mu)}\rangle)\rangle\rangle \tag{43}$$

$$=\frac{1}{N_r}\sum_{\mu=1}^{N_r}F\left(\frac{1}{N}\sum_{i=1}^{N}w_i^{(\mu)}\right), \tag{44}$$

with

$$w_i^{(\mu)}=w_i^{(\mu)}(t)=\sum_l\sum_n\Theta(T_b/2-|t-t_{oin}^{(\mu)}|)\Delta(t-lT_b), \tag{45}$$

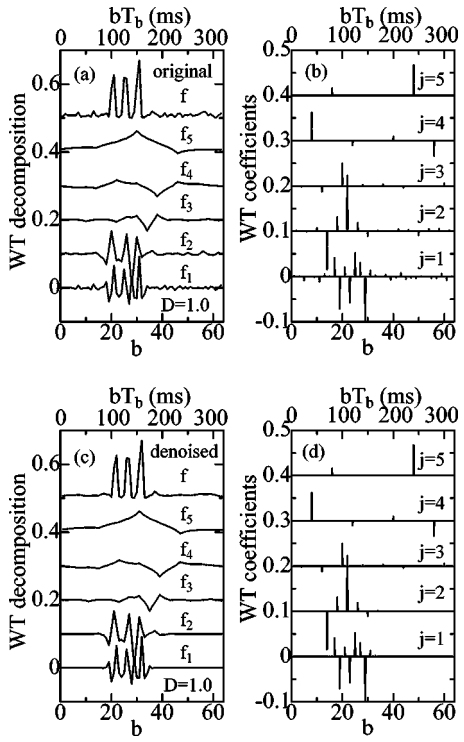

FIG. 14. (a) The original output signal $f=W_o$ (uppermost frame) for $D=1.0$ and $M=3$ with WT decomposition: $f\simeq\Sigma_{j=1}^{5}f_j$, and (b) its WT expansion coefficients c_{jk}. (c) The denoised output signal (uppermost frame) with WT decomposition, and (d) its denoised WT expansion coefficients c_{jk}^{dn} denoised with the parameters of $j_c=3$ and $\delta b=5$. Same as in Fig. 13.

where $\langle\langle\,\rangle\rangle$ and $\langle\,\rangle$ stand for averages over trials and an ensemble neurons, respectively, defined by Eq. (44), $t_{oin}^{(\mu)}$ is the nth firing time of the neuron i in the μth trial, $w_i^{(\mu)}(t)$ is its output signal of the neuron i with a time bin of T_b, and $F(y(t))$ is a functional of a given function of $y(t)$ relevant to a calculation of γ (or SNR). Figures 8(a) and 8(b) show that the relation $X(100,1)>X(1,100)$, namely,

$$F(\langle w_i^{(1)}\rangle)>\langle\langle F(w_1^{(\mu)})\rangle\rangle, \tag{46}$$

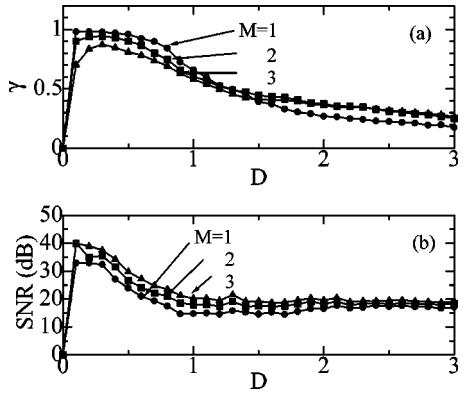

FIG. 15. (a) The cross correlation γ and (b) SNR as a function of D for $M=1$ (circles), $M=2$ (squares), and $M=3$ (triangles).

holds for our γ (or SNR). Note that if $F(\cdot)$ is linear, we get $X(100,1)=X(1,100)$ [Eq. (44)]. This implies that the inequality given, Eq. (46), is expected to arise from a *nonlinear* character of $F(\cdot)$. This reminds us of the algebraic inequality: $f(\langle x\rangle)\geqslant\langle f(x)\rangle$ valid for a convex function $f(x)$, where the bracket $\langle\cdot\rangle$ stands for an average over a distribution of a variable x. It should be again noted that there is no couplings among our neurons in the adopted model. Then the enhancement of SNR with increasing N is only due to a population of neurons. This is quite different from the result of some studies [34,35,38,39] in which the transmission fidelity is enhanced not only by noises but also by introduced couplings among neurons in an ensemble.

In our simulations reported in Sec. III, independent noises are applied to ensemble neurons. If instead we try to apply the same or *completely correlated* noise to them, which is equivalent to applying noises to a single neuron, an appreciable SR effect cannot be realized as discussed above. Then SR for transient spikes requires independent noises to be applied to a large-scale ensemble of neurons. This is consistent with the result of Liu, Hu, and Wang [39] who discussed the effect of correlated noises on SR for stationary analog inputs.

Although spike trains with small values of $M=1$ to 3 have been investigated in Sec. III, we can make an analysis of spikes with larger M or bursts, by using our method. In order to demonstrate its feasibility, we have made simulations for transient spikes with larger M. The upper curve of Fig. 16(a) expresses input $W_i(t)$ with a $M=7$ spike train whose firing times are $t_{im}=100$, 115, 130, 145, 160, 180, and 200 ms, and ISIs are $T_i=15$ and 20 ms. Firings of 100 neurons in an ensemble are depicted by raster in Fig. 16(b), where the parameters of $g_s=0.06$, $D=1.0$, and $N=100$ are adopted. The lower curve in Fig. 16(a) shows its output $W_o(t)$ averaged over the ensemble. We apply WT to $W_o(t)$ to get its WT coefficients and its WT decomposition, the latter being shown in Fig. 16(c). The $j=1$ and $j=2$ components are dominant. After the denoising, we get $\gamma=0.523$ and SNR=18.6 dB, which are comparable to those for $D=1.0$ with $M=1-3$ shown in Figs. 15(a) and 15(b). In our denoising method given by Eqs. (38) and (39), we extract noises outside the b region relevant to a cluster of spikes, but do not take into account the noises between pulses. When a number of pulses M and/or input ISI (T_i) become larger, a contribution from noises between pulses become considerable, which requires to modify the denoising method such as to extract noises between pulses, for example, as given by

$$c_{jk}^{dn}=c_{jk}, \quad \text{for} \quad j\geqslant j_c \quad \text{or} \quad k_{Lm}\leqslant k\leqslant k_{Um} \quad (m=1-M)$$
$$=0 \qquad \text{otherwise.} \tag{47}$$

In Eq. (47) k_{Lm} and k_{Um} are m and j dependent lower and upper limits given by

$$k_{Lm}=2^{-j}(t_{om}/T_b-\delta b), \quad k_{Um}=2^{-j}(t_{om}/T_b+\delta b), \tag{48}$$

where t_{om} is the mth firing time for the noise free and suprathreshold input and δb the margin of b.

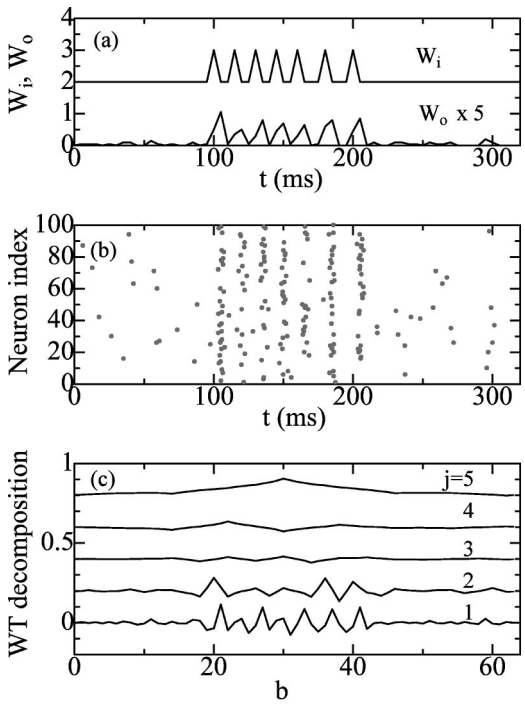

FIG. 16. (a) The input spike train $W_i(t)$ (upper curve) consisting of $M=7$ pulses, and its output signal $W_o(t)$ multiplied by a factor of 5 (lower curve) for $g_s=0.06$, $D=1.0$, and $N=100$, $W_i(t)$ being shifted upward by 2.0. (b) Raster showing firings of 100 neurons. (c) The WT decomposition: $f=W_o(t)\simeq\Sigma_{j=1}^{5}f_j$, results for $j=2$, 3, 4, and 5 being successively shifted upward by 0.2.

To summarize, the response of ensemble HH neurons to transient spike-train signals has been discussed with the use of the WT for subthreshold and suprathreshold inputs. The transmission for subthreshold transient inputs has been shown to be much improved by weak noises in large-scale ensemble neurons (SR effect): a population of neurons plays an essential role in SR for transient inputs. On the contrary, our simulation has shown that for suprathreshold transient inputs, the transmission fidelity evaluated by the cross-correlation and SNR is not enhanced by noises, in accordance with the previous study on SR for an aperiodic signal in ensemble FN neurons [33]. Quite recently, however, Stocks and Mannella have demonstrated SR for suprathreshold inputs in ensemble FN neurons [35], applying an aperiodic Gaussian signal with independent Gaussian noises to evaluate the mutual information. Suprathreshold SR (SSR) relies on the distributed nature of an aperiodic Gaussian signal and the mutual information adopted as a measure for information transmission. Actually, for a suprathreshold aperiodic Gaussian signal, the enhancement is realized in the mutual information but *not* in SNR, as pointed out in Ref. [81]. Thus the difference between the absence of SSR in our study and in Ref. [33] and the presence of SSR in Ref. [35] arises from the difference in an applied signal (a transient spike signal and a slow varying aperiodic signal [33] versus aperiodic Gaussian signal [35]) and in an evaluation method of information transmission (SNR and the cross correlation [33] versus the mutual information [35]). In an earlier paper of one of the authors (Stocks) [82], multiple threshold levels have been introduced to parallel arrays in order to get SSR, although in the later papers [35,81], threshold levels are set to the same value. Our preliminary calculation has shown that when we include the distribution of synaptic conductance g_s around the threshold level of g_{th} imitating the multithreshold systems [82], a weak SSR may be realized in cross-correlation and SNR. It would be possible that maximum SNR coincides with maximum mutual information because our approach considers signal fidelity rather than information processing. Details will be reported in a separate paper.

Our paper entirely relies on numerical simulations. I am currently trying to work on the theoretical description of the result reported in this paper. Conventional approaches having been employed for a study of SR such as the rate equation and linear-response theories [22,23], do not work in our case. Mato [46] adopted Gammaitoni's approach [83] for an analysis of his SR result with the continuous spike-train signals. It seems, however, not to be translatable directly to our case of transient spike-train signals even if our HH model is replaced by a simpler IF model or threshold-crossing model. Its analytical study is left as our future problem.

Note added in proof. Recently, a semianalytical, dynamical mean-field theory has been developed [84], which may elucidate the mechanism of an improvement of the transmission fidelity by increasing the size of neuron ensembles.

ACKNOWLEDGMENT

This work was partly supported by a Grant-in-Aid for Scientific Research from the Japanese Ministry of Education, Culture, Sports, Science and Technology.

[1] F. Rieke, D. Warland, R. Steveninck, and W. Bialek, *Exploring the Neural Code* (MIT Press, Cambridge, 1996).
[2] R. C. deCharms, Proc. Natl. Acad. Sci. U.S.A. **95**, 15166 (1998).
[3] J. J. Eggermont, Neurosci. Biobehav Rev. **22**, 355 (1998).
[4] W. M. Ursey and R. C. Reid, Annu. Rev. Physiol. **61**, 435 (1999).
[5] R. C. deCharms and A. Zador, Annu. Rev. Neurosci. **23**, 613 (2000).
[6] A. Pouget, P. Dayan, and R. Zemel, Nat. Neurosci. **1**, 125 (2000).
[7] E. D. Adrian, J. Physiol. (London) **61**, 49 (1926).
[8] N. Suga, W. E. O'Neill, K. Kujirai, and T. Manabe, J. Neurophysiol. **49**, 1573 (1983).
[9] M. Konishi, Harvey Lect **86**, 47 (1992).
[10] C. E. Carr, W. Heiligenberg, and G. J. Rose, J. Neurosci. **6**, 107 (1986).
[11] R. Eckhorn, R. Bauer, W. Jordan, M. Brosch, W. Kruse, M.

Munk, and H. J. Reitboeck, Biol. Cybern. **60**, 121 (1988).
[12] C. M. Gray and W. Singer, Proc. Natl. Acad. Sci. U.S.A. **86**, 1698 (1989).
[13] E. T. Rolls and M. J. Tovee, Proc. R. Soc. London, Ser. B **257**, 9 (1994).
[14] S. Thorpe, D. Fize, and C. Marlot, Nature (London) **381**, 520 (1996).
[15] J. J. Hopfield, Nature (London) **376**, 33 (1995).
[16] D. Horn and S. Levanda, Neural Comput. **10**, 1705 (1998).
[17] R. van Rullen and S. J. Thorpe, Neural Comput. **13**, 1255 (2001).
[18] R. C. deCharmes and M. M. Merzenich, Nature (London) **381**, 610 (1996).
[19] R. D. Traub, M. A. Whittington, and J. G. R. Jefferys, Neural Comput. **9**, 1251 (1997).
[20] N. Hatsopoulas, C. L. Ojakangas, L. Paninski, and J. P. Donohue, Proc. Natl. Acad. Sci. U.S.A. **95**, 15706 (1998).
[21] Z. F. Mainen and T. J. Sejnowsky, Science **268**, 1503 (1995).
[22] L. Gammaitoni, P. Hänngi, P. Jung, and F. Marchesoni, Rev. Mod. Phys. **70**, 223 (1998).
[23] V. S. Anishchenko, A. B. Neiman, F. Moss, and L. Schimansky-Geier, Usp. Fiz. Nauk **169**, 7 (1999) [Sov. Phys. Usp. **42**, 7 (1999)].
[24] A. R. Bulsara, T. C. Elston, C. R. Doering, S. B. Lowen, and K. Lindenberg, Phys. Rev. E **53**, 3958 (1996).
[25] H. E. Plesser and S. Tanaka, Phys. Lett. A **225**, 228 (1994).
[26] T. Shimokawa, K. Pakdaman, and S. Sato, Phys. Rev. E **59**, 3427 (1999).
[27] A. Longtin, J. Stat. Phys. **70**, 309 (1993).
[28] K. Wiesenfeld, D. Pierson, E. Pantazelou, C. Dames, and F. Moss, Phys. Rev. Lett. **72**, 2125 (1994).
[29] A. Longtin and D. R. Chialvo, Phys. Rev. Lett. **81**, 4012 (1994).
[30] S. G. Lee and S. Kim, Phys. Rev. E **60**, 826 (1999).
[31] T. Shimokawa, A. Rogel, K. Pakdaman, and S. Sato, Phys. Rev. E **59**, 3461 (1999).
[32] B. Lindner and L. Schimansky-Geier, Phys. Rev. Lett. **86**, 2934 (2001).
[33] J. J. Collins, C. C. Chow, and T. T. Imhoff, Nature (London) **376**, 236 (1995).
[34] T. Kanamaru, T. Horita, and Y. Okabe, Phys. Rev. E **64**, 31908 (2000).
[35] N. G. Stocks and R. Mannella, Phys. Rev. E **64**, 30902 (2001).
[36] X. Pei, L. Wilkens, and F. Moss, Phys. Rev. Lett. **77**, 4679 (1996).
[37] S. Tanabe, S. Sato, and K. Pakdaman, Phys. Rev. E **60**, 7235 (1999).
[38] Y. Wang, D. T. W. Chik, and Z. D. Wang, Phys. Rev. E **61**, 740 (2000).
[39] F. Liu, B. Hu, and W. Wang, Phys. Rev. E **63**, 31907 (2000).
[40] J. K. Douglass, L. Wilkens, E. Pantazelou, and F. Moss, Nature (London) **365**, 337 (1993).
[41] X. Pei, L. A. Wilkens, and F. Moss, J. Neurophysiol. **76**, 3002 (1996).
[42] J. E. Levins and J. P. Miller, Nature (London) **380**, 165 (1996).
[43] B. J. Gluckman, T. I. Netoff, E. J. Neel, W. L. Ditto, M. L. Spano, and S. J. Schiff, Phys. Rev. Lett. **77**, 4098 (1996).
[44] D. Nozaki, D. J. Mar, P. Grigg, and J. J. Collins, Phys. Rev. Lett. **82**, 2402 (1999).
[45] F. Chapeau-Blondeau, X. Godivier, and N. Chambet, Phys. Rev. E **53**, 1273 (1996); X. Godivier and F. Chapeau-Blondeau, Europhys. Lett. **35**, 473 (1996).
[46] G. Mato, Phys. Rev. E **58**, 876 (1998); **59**, 3339 (1999).
[47] H. Hasegawa, e-print cond-mat/0202252.
[48] J. J. Collins, C. C. Chow, and T. T. Imhoff, Phys. Rev. E **52**, R3321 (1995); **54**, 5575 (1996).
[49] R. Fakir, Phys. Rev. E **57**, 6996 (1998); **58**, 5175 (1998).
[50] R. D. Traub, J. G. R. Jefferys, and M. A. Whittington, *Fast Oscillations in Cortical Circuits* (MIT Press, Cambridge, 1999).
[51] W. E. Sullivan and M. Konishiki, J. Neurosci. **393**, 268 (1998).
[52] G. Rose and W. Heilingenberg, Nature (London) **318**, 178 (1985).
[53] I. Daubechies, *Ten Lectures on Wavelets*, CBMS-NSF Regional Conference on Series on Applied Mathematics (Soc. Ind. Appl. Math, Philadelphia, 1992), Vol. 61.
[54] For reviews on the WT and its application see: N. M. Astaf'eva, Usp. Fiz. Nauk **166**, 1145 (1996) [Phys. Usp. **39**, 1085 (1996)]; I. M. Dremin, O. V. Ivanov, and V. A. Nechitailo, e-print hep-ph/0101182.
[55] V. J. Samar, A. Bopardikar, R. Rao, and K. Swartz, Brain Lang. **66**, 7 (1999).
[56] S. Blanco, C. E. D'Attellis, S. I. Isaacson, O. A. Rosso, and R. O. Sirne, Phys. Rev. E **54**, 6661 (1996).
[57] S. Blanco, A. Figliola, R. QuianQuiroga, O. A. Rosso, and E. Serrano, Phys. Rev. E **57**, 932 (1998).
[58] J. Ratz, L. Dickerson, and B. Turetsky, Brain Lang. **66**, 61 (1999).
[59] L. J. Trejo, and M. J. Shensa, Brain Lang. **66**, 89 (1999).
[60] T. Demiralp, A. Ademoglu, M. Schürmann, C. Başar-Eroglu, and E. Başar, Brain Lang. **66**, 108 (1999).
[61] T. Demiralp, J. Yordanova, V. Kolev, A. Ademoglu, M. Devrin, and V. J. Samar, Brain Lang. **66**, 29 (1999).
[62] O. A. Rosso, S. Blanco, J. Yordanova, V. Kolev, A. Figliola, M. Schürmann, E. Başar, J. Neurosci. Methods **105**, 65 (2001).
[63] E. Hulata, R. Segev, Y. Shapira, M. Benveniste, and E. Ben-Jacob, Phys. Rev. Lett. **85**, 4637 (2000).
[64] J. C. Letelier and P. P. Weber, J. Neurosci. Methods **101**, 93 (2000).
[65] G. Zouridakis and D. C. Tam, Comput. Biol. Methods **27**, 9 (1997).
[66] D. Stratimirović, S. Milosević, S. Blesić, and M. Ljubiavljević, Physica A **291**, 13 (2001).
[67] H. Hasegawa, e-print cond-mat/0109444.
[68] A. Destexhe, Z. F. Mainen, and T. J. Sejnowski, in *The Handbook of Brain Theory and Neural Networks*, edited by M. A. Arbib (MIT Press, Cambridge, 1998), p. 956.
[69] R. G. Smith, in *The Handbook of Brain Theory and Neural Networks*, edited by M. A. Arbib (MIT Press, Cambridge, 1998), p. 816.
[70] M. N. Shadlen and W. T. Newsome, Curr. Opin. Neurobiol. **4**, 569 (1994).
[71] H. Hasegawa (unpublished).
[72] A. L. Hodgkin and A. F. Huxley, J. Physiol. **117**, 500 (1952).
[73] C. Morris and H. Lecar, Biophys. J. **35**, 193 (1981).
[74] E. A. Bartnik, K. J. Blinowska, and P. J. Durks, Biol. Cybern. **67**, 175 (1992).
[75] O. Bertrand, J. Bohorquez, and J. Pemier, IEEE Trans. Biomed. Eng. **41**, 77 (1994).
[76] D. L. Donoho, I. M. Johnstone, and B. W. Silverman, IEEE

Trans. Inf. Theory **41**, 613 (1995).
[77] R. Q. Quiroga, Physica D **145**, 278 (2000).
[78] S. Haykin, in *The Handbook of Brain Theory and Neural Networks*, edited by M. A. Arbib (MIT Press, Cambridge, 1998), p. 82.
[79] H. Hasegawa, Phys. Rev. E **61**, 718 (2000); **62**, 1456(E) (2000); Bull. Tokyo Gakugei Univ. Ser. 4, **53**, 31 (2001).
[80] W. H. Press, S. A. Teukolsky, W. T. Vetterling, and B. P. Flannery, *Numerical Recipes in Fortran*, 2nd. ed. (Cambridge University Press, New York, 1992), p. 584.
[81] N. G. Stocks, Phys. Rev. E **63**, 41114 (2001).
[82] N. G. Stocks, Phys. Rev. Lett. **84**, 2310 (2000).
[83] L. Gammaitoni, Phys. Rev. E **52**, 4691 (1995).
[84] H. Hasegawa, e-print cond-mat/0206135.